The X-ray Structure of A399 and A401: A Pre-Merging Cluster Pair

Yutaka Fujita[1,2], Katsuji Koyama[3], Takeshi Tsuru[3], and Hironori Matsumoto[3]

[1]*Graduate School of Human and Environmental Studies*
Kyoto University, Kyoto 606-01, Japan

[2]*Yukawa Institute for Theoretical Physics*
Kyoto University, Kyoto 606-01, Japan

E-mail(YF) fujita@yukawa.kyoto-u.ac.jp

[3]*Department of Physics, Faculty of Science*
Kyoto University, Kyoto 606-01, Japan

Subject headings: Galaxies: Clustering - Galaxies: clusters: individual: (A399, A401) - X-rays: Galaxies

Abstract

We present *ASCA* results of the pair clusters A399 and A401. The region between the two clusters exhibits excess X-rays over the value expected with a simple superposition of the two clusters. We see, however, no temperature rise at the merging front; the temperature is near the average of those in the inner regions of the two clusters. These indicate that the two clusters are really interacting but it is not strong at present. The inner regions of the two clusters show no radial variations of temperature, abundance and absorption values. We set upper-limits of mass deposition rate of cooling flow to be $\dot{M} < 35\ \mathrm{M_\odot yr^{-1}}$ and $\dot{M} < 59\ \mathrm{M_\odot yr^{-1}}$ for A399 and A401, respectively. A hint of azimuthal variation of the temperature is also found.

1 INTRODUCTION

A large fraction of clusters of galaxies have been found to contain substructures in the optical galaxy distributions and X-ray surface brightness. This may be understood in the framework of the hierarchical clustering scenario; clusters of galaxies evolve by accreting other clusters or smaller groups of galaxies. By the merging, the volume or density of the X-ray emitting gas may increase, hence X-ray luminosity increases as clusters evolve. Gioia et al.(1990) and Edge et al. (1990), for example, reported evidence for the luminosity evolution of the X-ray emitting intracluster gas. Recent observations with *ROSAT* provide more direct evidence for the cluster merging; in some clusters, their X-ray surface brightness distributions are shifted from the galaxy number density distribution, in which local high temperature regions are found. These indicate that the clusters are actually merging with a strong shock at the merging front (Henry & Briel 1995 ; Zabludoff & Zaritsky 1995 ; Burns et al. 1995). Suppose that the subcluster components are more separated, then the cluster may not be regarded as a single cluster but would be counted as two separate clusters. The distinction may be somewhat ambiguous; it depends on the projected distance of the clusters. If the system is gravitationally bounded, then the clusters will merge and evolve to a single, richer cluster in the future.

The pair of A399 and A401 is one of the closest and the brightest pair clusters, hence would be the best candidate of pre-merging clusters. Karachentsev and Kopylov (1980) measured the velocity dispersions and mean radial velocities of the two clusters and concluded that

these data are consistent with the pair being gravitationally bound. However, although several studies have been made on the pair clusters, whether they are thermally interacting or not is still open problem.

Some authors claimed that they may be interacting. McGlynn & Fabian (1984) pointed out that their lack of cooling flows may be due to the interaction. Although both of these two clusters possess luminous cD galaxies, their cooling flows are relatively weak (McGlynn & Fabian 1984). By numerical simulations of cluster collisions, they confirmed that, at the first encounter, one cluster can even pass through the other without destroying the optical components, while the intracluster gas is largely affected and hence cooling flows, if any, may be disrupted (McGlynn & Fabian 1984). Furthermore, A401 is one of only a few rich clusters that is report to have an extensive cluster radio halo (Harris, Kapahi, & Ekers. 1980 ; Roland et al. 1981). Harris et al. (1980) suggested that radio halos form during the coalescence of clusters.

On the other hand, X-ray observation with the *Einstein* satellite indicated that the emission between the two clusters is explained by the simple superposition of the extended emission from the two clusters (Ulmer & Cruddace 1981).

We report, for the first time, spatially resolved X-ray spectra of the pair A399 and A401 with the *ASCA* satellite. We found evidence for the interaction between these two clusters; there is an excess X-ray emission in the middle of the two clusters above the expected flux from the simple superposition of the two clusters. We also discuss large-scale temperature variations in the outer regions of the two clusters, which may be affected by the interaction between them.

We describe the observations and the data reduction in section 2 and the analysis and the results in section 3. Then, in section 4, we discuss the structure of the two clusters and the interaction between them based on the results. Section 5 is devoted to conclusions. We assume $H_0 = 50 \mathrm{kms}^{-1}\mathrm{Mpc}^{-1}$ and $q_0 = 0.5$ through out this paper.

2 Observations and Data reduction

We observed A399, A401 and the region between the two clusters (hereafter we call it the link-region) with the *ASCA* satellite on 16, 18 and 17 August 1994, respectively. We rejected data at low elevation angles from bright earth ($< 20^\circ$) and those affected by South Atlantic Anomaly. Hot and flickering pixels for the SIS data were removed. The rise-time rejection technique was used to reject particle events in the GIS data. After these data screening, the accumulation times for A399, A401 and the link-region are 2.6×10^4s, 2.9×10^4s and 3.5×10^4s, respectively. Figure 1 shows GIS image of the two clusters; a mosaic map of the three pointing observations in which corrections for both the exposure time and telescope vignetting are made. We divided the observed regions symmetrically to the line connecting the centers of the two clusters as are illustrated in figure 1, and made separate spectra from each region. Central regions of A401 and A399 (within $6'$ radius from the X-ray peak of each cluster) are denoted as A0 and B0, respectively, while the regions of C0 and D are located between the two clusters with radius of $6'$ and $10'$, respectively. The center positions of regions A0, B0, C0 and D are listed in table 1, together with the optical centers (the positions of the cD galaxies: Hill & Oegerle

1993) of A399 and A401. Quadrants of the annulus around the regions of A0, B0 and C0, with $6'$ inner and $18'$ of outer radius are assigned as A1-A4, B1-B4 and C1-C2, respectively. We further divided the inner regions A0 and B0 into 6 annulus with $1'$ interval, and made separate spectra. The SIS spectra are only available for the regions of A0, B0 and D, because a large fraction of the other regions are outside of the SIS field of view, and because the poor sensitivity at the high energy of SIS makes it hard to obtain reliable wide-band X-ray spectra in the outer regions of the clusters. The spectra in the series A and B were made using the data of the pointings centered on A399 and A401, respectively, while those in the series C and D were derived from the pointing data at the link-region. The background spectra were made using the averaged blank field data provided by *ASCA* group, from the same detector positions as the on-source spectra. Then the background subtractions were made after correcting the exposure time. For the image analysis, we have used an improved response function of *ASCA* telescope provided by the XRT hardware team (Shibata, Honda, & Hirayama, private communication), in which energy dependent point spread function and effective area are taken into account. In fact, the ray-tracing simulation demonstrated that the error of the observed temperature is $< 10\%$ in the relevant temperature of 5-10 keV (Shibata, Honda, & Hirayama, private communication). Stray light from the two clusters in region C0 is also estimated to be $< 30\%$ of the observed flux in the region (Honda, private communication).

3 Analysis and Results

The background subtracted spectra were binned to contain > 20 counts for each energy bin; minimum counts for which χ^2 statistics can be applied, and then fitted to a thin thermal Raymond & Smith model (1977) plus an interstellar absorption using the XSPEC package. The spectra from GIS2 and GIS3 or SIS0 and SIS1 were simultaneously fitted with separate response functions and independent normalization factors for each detector. We show some examples of GIS and SIS results separately in figures 2 and 3; the GIS and SIS spectra and their best-fit model curves in the regions of A0, B0 and C0 (for SIS, the spectrum is from the region D). In all the regions, these models were found to be acceptable with the best-fit reduced χ^2 values in the range of 0.8 - 1.1 for the GIS data and 1.0 - 1.5 for the SIS data. The best-fit parameters are listed in tables 2 and 3.

The best-fit parameters obtained with the GIS and SIS spectra agree well with each other, except for absorption column densities, $N_{\rm H}$. These are derived essentially from the spectral below 1 keV. In this energy band, SIS is more sensitive than GIS, hence the SIS results would be more reliable. However, we notice here that calibration errors in the low energy band give some bias to the estimated values. Therefore the absolute absorption may have systematic error, if it is less than a few times $10^{21}{\rm cm}^{-2}$, which is the case of the present observations. Nevertheless, we can reliably compare relative values of $N_{\rm H}$ from the SIS. The relative values of $N_{\rm H}$ are almost constant from position to position. Therefore, we regard that the absolute $N_{\rm H}$ is also constant everywhere in our fields. The $N_{\rm H}$ values determined

with SIS are a few times larger than that of the galactic absorption, which is 1.1×10^{21} cm^{-2} (The Einstein On Line Service, Smithsonian Astrophysical Observatory). However, as we already noted, they are within the calibration errors, hence we do not discuss further for the $N_{\rm H}$ structure.

3.1 Radial Structure

In figures 4 and 5, we show radial profiles of the temperature of A399 and A401, respectively, in which inner $6'$ regions are divided to 6 annulus of $1'$ interval, while the data of $6' - 18'$ are averages of A1-A4 and of B1-B4, for the A399 and A401, respectively. Uncertainty ranges of the fit given in the figures are 90% confidence (hereafter errors are 90% confidence unless otherwise mentioned). We see no significant radial variations of the temperature in the inner regions. As already noted, we see no variations of the $N_{\rm H}$ value (SIS data), neither. These indicate that no significant cooling flow components exist around the cD galaxies. We further studied the SIS data, because SIS has better sensitivity than GIS at the energy of relevant temperature of the cooling flows. In order to find upper limits of the cooling flows we fit the SIS spectra from the whole regions of A0 and B0 to a thin thermal plasma model (Raymond & Smith 1977) plus an absorption. We have fixed the temperature, abundance and absorption column density to their best-fit values and added a cooling flow component model as described in Mushotzky & Szymkowiak (1988), in which the cooling is assumed to start from the temperature of the ambient intracluster gas. We thus estimate that the flow rates of the cooling gas are $\dot{M} < 35$ M$_\odot$yr^{-1} for A399 and $\dot{M} < 59$ M$_\odot$yr^{-1} for

A401.

The average temperature in the central regions within $6'$ are found to be 6.9 keV and 8.0 keV, for A399 and A401, respectively (figure 1, table 3). Moving to the larger radius of $6' - 18'$, the average temperatures show slight increases for both the clusters; from 6.9 keV to 8.1 keV and from 8.0 keV to 9.3 keV, for A399 and A401, respectively. However the 90% errors overlap with each other and the calibration of *ASCA* would be still incomplete. Thus we cannot argue the temperature rise in the radial direction is real.

We investigated the abundance distributions of A399 and A401 as a function of radius, and found no significant radial variations, although the errors are large.

Thus, together with the global isothermality as discussed above, the intracluster plasma near the cluster centers would be rather uniform.

3.2 The Link-region

In order to see whether there are excess X-rays or not in the link-region, in figure 6, we plotted a photon flux profile along the strip AA' with $5'$ width (see figure 1). Assuming right-left symmetry of the flux distribution at the positions of cD galaxies for each cluster, we show, with the dotted lines in figure 6, possible contributions of A401 and A399 to the link region. We clearly found excess X-rays in the link-region. Further support of the excess emission is found in the energy fluxes of regions A1, A3, B1 and B3 as are listed in table 3. The fluxes are of the best-fit parameters in table 3 for various regions. They are corrected for vignetting and background. The sum of the energy fluxes

of A3 and B3 is $F_{33} = 11.0 \times 10^{-12}$erg cm^{-2}s^{-1}, and the sum of the energy fluxes of A1 and B1 is $F_{11} = 6.3 \times 10^{-12}$erg cm^{-2}s^{-1}. If the two clusters were spherically symmetric and they were simply superposed on the line of sight, the sum of the expected energy flux contribution of A399 in B3 and that of A401 in A3 would be $\tilde{F_{33}} \simeq 2^{-3} \times F_{11}$, because the X-ray surface brightness distribution in the outer region of a typical cluster is well fitted by r^{-3}. The fact $F_{33} > F_{11} + \tilde{F}_{33}$ indicates that the the two clusters are physically interacting. In figure 7, we present the best-fit temperature distribution along the major axis. The temperature shows slow decrease from A401 to A399, and that of the rink-region is in the average value of A401 and A399. The abundance distribution is also examined, but is unclear due to its large errors.

3.3 Non radial Structure

The best-fit temperatures in the quadrants of the outer cluster regions and the average values in the inner regions (A0 and B0) are shown in figures 1. We found that the temperature of the outer regions is, in average, higher than those in the inner regions in both the clusters, as already noted. We further found a signature of non radial temperature variations in A399, although we can reject the isothermal model at most at the 80% confidence level. We note that the calibration errors in azimuthal direction are small compared with those in in radial direction. As for the abundance, relative large errors prevent us to say definite statements.

4 DISCUSSION

The previous *Einstein* MPC results show that the 2 - 10 keV fluxes of A399 and A401 is 3.4×10^{-11}ergcm^{-2}s^{-1} and 5.9×10^{-11}ergcm^{-2}s^{-1}, respectively, and their temperatures are 6.0 keV and 8.6 keV , respectively (Edge et al. 1990 ; David et al. 1993). We determine the 2 - 10 keV fluxes of A399 and A401 within $18'$ (about 2 Mpc) to be 3.0×10^{-11}erg cm^{-2}s^{-1} and 5.7×10^{-11}erg cm^{-2} s^{-1}, which is in excellent agreement to that determined with *Einstein*. The mean temperatures determined with *ASCA* of about 6.9 and 8.0 keV agree also well to the *Einstein*. The inferred temperature and luminosity fit well to the empirical correlation given by David et al.(1993).

We found no significant radial variations in the central regions ($< 6' = 0.8$ Mpc) of the clusters. This, however, does not immediately indicate that the radial structure of iron found within about 100 kpc in the Centaurus and Virgo clusters is absent in A401 or A399, because the distance to the two clusters gives angular distance of $1'$, the spatial resolution of *ASCA*, to be 130kpc (Fukazawa et al. 1994 ; Koyama et al. 1991). We found no signature of cooling flows for both the clusters, giving upper limits of the mass deposition rates of $\dot{M} < 35$ M$_\odot$yr^{-1} for A399 and $\dot{M} < 59$ M$_\odot$yr^{-1} for A401. These values are relatively small as for the clusters with cD galaxy (McGlynn & Fabian 1984).

The most important information of the present observation is the X-ray emission in the region between A401 and A399 clusters. Ulmer and Cruddace (1981) claimed that the Einstein data can be explained as the simple superposition of foreground (A399) and background (A401) extended emission of the clusters. We found clear

excess X-rays in the link-region over the value expected with a simple superposition of the two clusters.

Numerical simulations of Evrard (1990) and Schindler & Müller (1993) showed that during collision, gas between two clusters should be heated. This is not the case of our observation; the temperature in the link-region derived by *ASCA* is almost the same as those of A0 and B0. Furthermore, table 1 shows that the locations of the X-ray peaks and the cD galaxies in each cluster coincide within the error ($\sim 1'$). These facts support that interaction between A401 and A399 does exist, but no strong shock has not been made in the link-region. Thus we interpret that the cluster pair A401-A399 is currently in pre-merging phase. We guess that after several Gyr, the pair of the clusters will exhibit similar X-ray properties such as those of A754 and A2255, which are thought to be currently colliding (Henry & Briel 1995 ; Zabludoff & Zaritsky 1995 ; Burns et al. 1995). In A754, some regions have temperature of $T > 12$keV while in some other regions $T < 6$keV. In A754 and A2255, the locations of the brightest galaxies in the clusters are away from the X-ray peaks more than $1'$ (Henry & Briel 1995; Burns et al. 1995).

As for less possible scenario, although we cannot reject with the present result, is that the pair clusters is a relic of a past-strong collision. A recent numerical simulation in which parameters are taken from the observed values of A399 and A401 shows that after their collision, the temperature between the two clusters goes back to the initial value by an adiabatic expansion in $\sim 1 - 2$Gyr (Ishizaka 1995 private communication). The projection distance between A399 and A401 is 4.25Mpc (Karachentsev and Kopylov 1980) and their line-

of-sight velocity separation, $c\Delta z$, is $\sim 1000\mathrm{km\,s^{-1}}$. If we take these values as the real spatial separation and relative velocity, the time needed for the two clusters to separate as is observed is 4 Gyr and is well shorter than the Hubble time. Even if $H_0 = 100\mathrm{km\,s^{-1}\,Mpc^{-1}}$, the conclusion is the same. Their lack of cooling flows may favor the past strong interaction; with the strong interaction cooling flows were destroyed.

The spectra in outer regions of A399 may show azimuthal variations, although error bars are large. If they are true, these variations might be relics of the past-interaction between the two clusters, or might be made by interactions of possible subclusters in the cluster.

The high temperature found in the region A4 may reflect the generation of shock waves caused by the collision between the subclusters and the main clusters. However, figure 1 shows that there are no significant substructures except for the extensions toward the link-region.

An interpretation can be made that the variances reflect the relics of the gravitational perturbations at the cluster formation period, which have not grown up as significant subclusters; dark matter blobs which correspond to the perturbations would have collided into the central regions of the clusters, the gas trapped in them would have been shocked and the temperature would have risen.

5 CONCLUSION

We report *ASCA* X-ray observation of the pair clusters A399 and A401. No significant radial variations are found in the central regions of the two clusters. There is an emission excess in the region between

them (link-region) over the value expected with a simple superposition of the clusters. The temperature in it is not higher than that in the central regions of the clusters. In the outer regions of A399, signatures of azimuthal variation of temperature are found.

These results suggest that the two clusters are in a pre-merging phase; the interaction is not strong at present. We cannot exclude a past strong collision. We encourage more detailed observations and the comparison with numerical simulations.

We thank all of the members of the *ASCA* team and the launching staffs of the Institute of Space and Astronautical Science. We thank C. Ishizaka for providing simulation data.

REFERENCES

Burns, J. O., Roettiger, K., Pinkney, J., Perley, R. A., Owen, F. N., & Voges, W. 1995, ApJ., 446, 583

David, L. P., Slyz, A., Jones, C., Forman, W., & Vrtilek, S. D. 1993, ApJ., 412, 479

Edge, A. C., Stewart, G. C., Fabian, A. C., & Arnaud, K. A. 1990, Mon.Not R. astr.Soc., 245, 559

Evrard, A. E. 1990, in Clusters of Galaxies, ed. W. R. Oegerle, M. J. Fitchett, & L. Danly (Cambridge Univ. Press), 287

Fukazawa, Y., Ohashi, T., Fabian, A. C., Canizares, C. R., Ikebe, Y., Makishima, K., Mushotzky, R. F., & Yamashita, K. 1994, Pub.Astr.Soc.Japan, 46, L55

Gioia, I. M., Henry, J. P., Maccacaro, T., Morris, S. L., Stocke, J. T.,& Wolter, A. 1990, ApJ., 356, L35

Harris, D. E., Kapahi, V. K., & Ekers, R. D. 1980, Astron.Astrophys.Suppl., 39, 215

Henry, J. P., & Briel, U. G. 1995, ApJ., 443, L9

Hill, J. M., & Oegerle, W. R. 1993, AJ., 106, 831

Karachentsev, I. D., & Kopylov, A. I. 1980, Mon.Not.R.astr.Soc., 192, 109

Koyama, K., Takano, S., & Tawara, Y. 1991, Nature, 350, 135

McGlynn, T. A., & Fabian, A. C. 1984, Mon.Not.R.astr.Soc., 208, 709

Mushotzky, R. F., & Szymkowiak, A. E. 1988, in Cooling Flows in Clusters of Galaxies, ed. Fabian, A. C. (Kluwer Academic Publishers), 53

Raymond, J. C., & Smith, B. W. 1977, ApJS. 35, 419

Roland, J. H., Sol, H., Pauliny-Toth, I., & Witzel, A. 1981, Astron.Astrophys., 100, 7

Schindler, S., & Müller, E. 1993, Astron.Astrophys., 272, 137

Ulmer, M. P., & Cruddace, R. G. 1981, ApJ., 246, L99

Zabludoff, A. I., & Zaritsky, D. 1995, ApJ., 447, L21

Figure Captions

Fig.1. - The background-inclusive mosaic images taken with the GIS sensor, the configuration of the regions for spectral analysis (bold) and the best fit temperature (keV) observed with GIS (roman) and SIS (italic). Exposure and vignetting area corrected. The contours are drawn at 5, 8, 13, 21, 33, 52 and 84 counts s^{-1} $arcmin^{-2}$.

Fig.2. - X-ray spectra observed with two GIS. The histogram shows the best fitting (R - S plasma + absorption column density). (a) Region A0 (b) Region B0 (c) Region C0

Fig.3. - X-ray spectra observed with two SIS. The histogram shows the best fitting (R - S plasma + absorption column density). (a) Region A0 (b) Region B0 (c) Region D

Fig.4. - Profiles of temperature vs. the distance from the center of A399.

Fig.5. - The same as Fig.5 but for A401.

Fig.6. - The solid lines show the photon counts after the correction of exposure time and vignetting along the strip AA' (Fig.1). The dotted lines are reflection of the solid lines against to the center of the clusters. The dashed line indicates the background level.

Fig.7. - Profiles of temperature along the line which connects A399 and A401.

TABLE 1

LOCATIONS (2000)

	z	X-ray	cD[a]
A0(A399)	0.0715	2h57m53.25s, +13°02′39.26″	2h57m53.15s, +13°01′51.9″
B0(A401)	0.0748	2h58m58.97s, +13°34′57.35″	2h58m57.88s, +13°34′59.1″
C0 and D	...	2h58m30.87s, +13°18′14.36″	...

a. Hills & Oegerle 1993.

Fig.1a

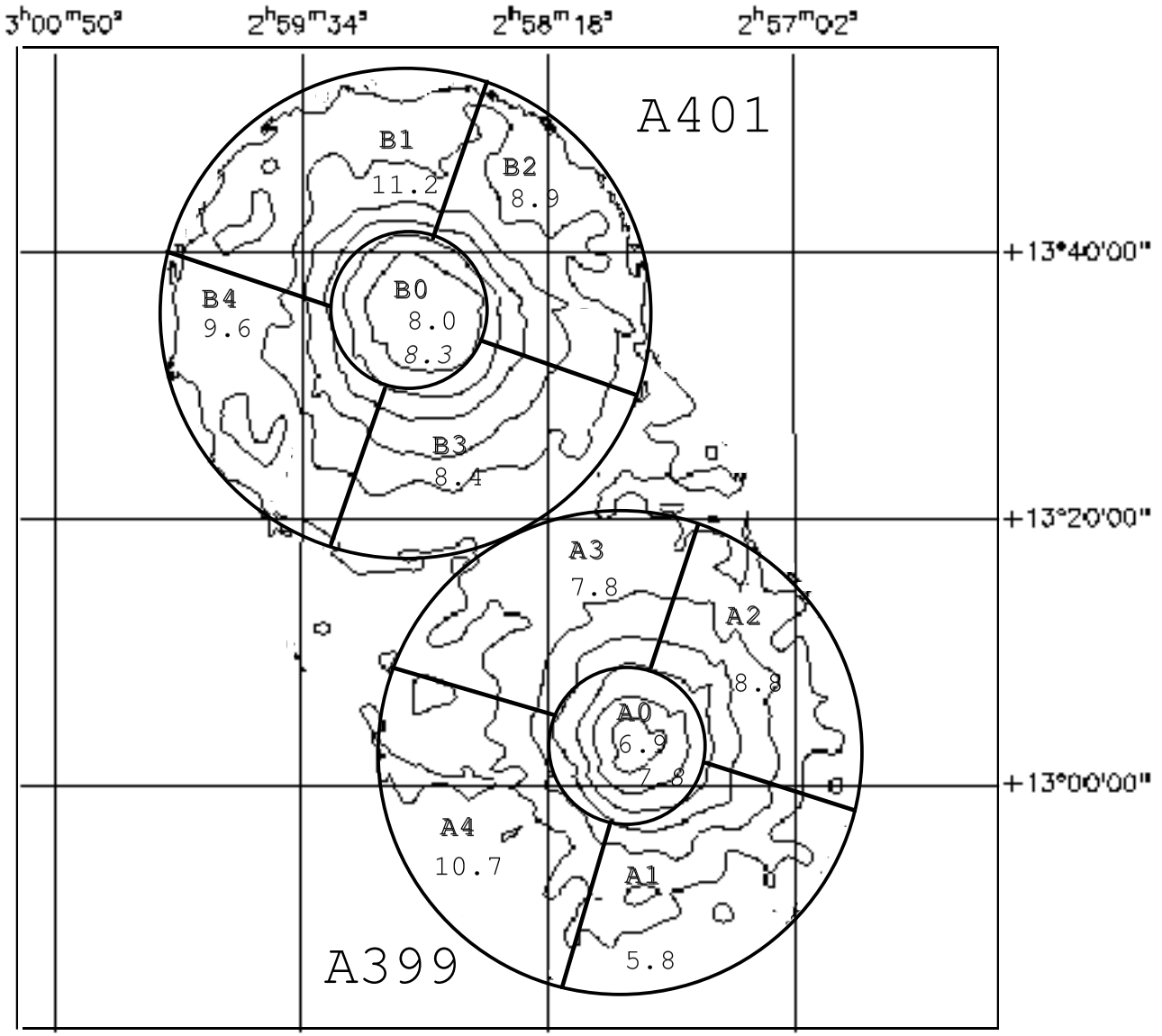
3h00m50s
2h59m34s
2h58m18s
2h57m02s
+13°40'00"
+13°20'00"
+13°00'00"
A401
B1
11.2
B2
8.9
B0
8.0
8.3
B4
9.6
B3
8.4
A3
7.8
A2
8.8
A0
6.9
7.8
A4
10.7
A1
5.8
A399

Fig.1b

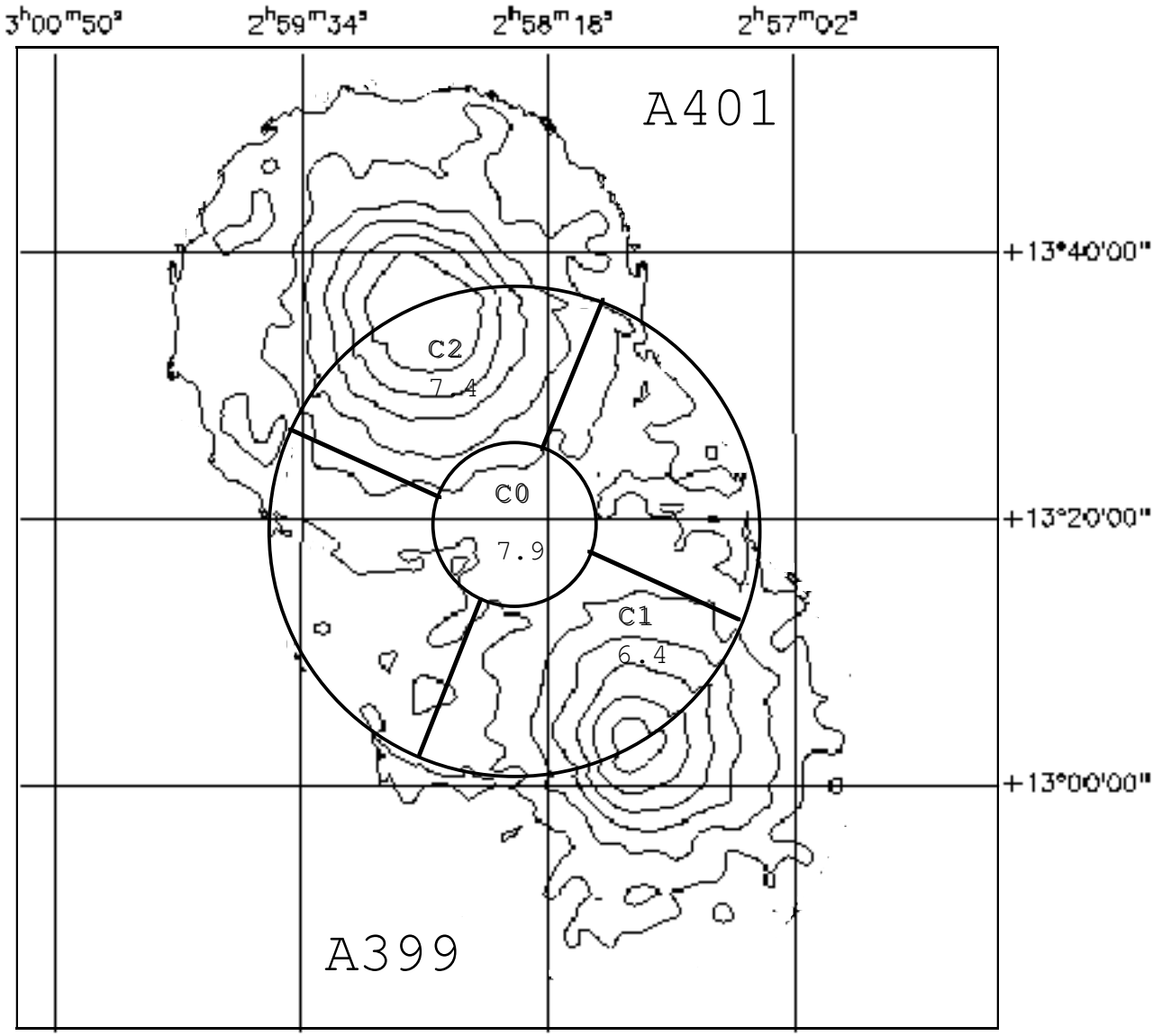
3h00m50s
2h59m34s
2h58m18s
2h57m02s
A401
+13°40'00"
+13°20'00"
+13°00'00"
C2
7.4
C0
7.9
C1
6.4
A399

Fig.1c

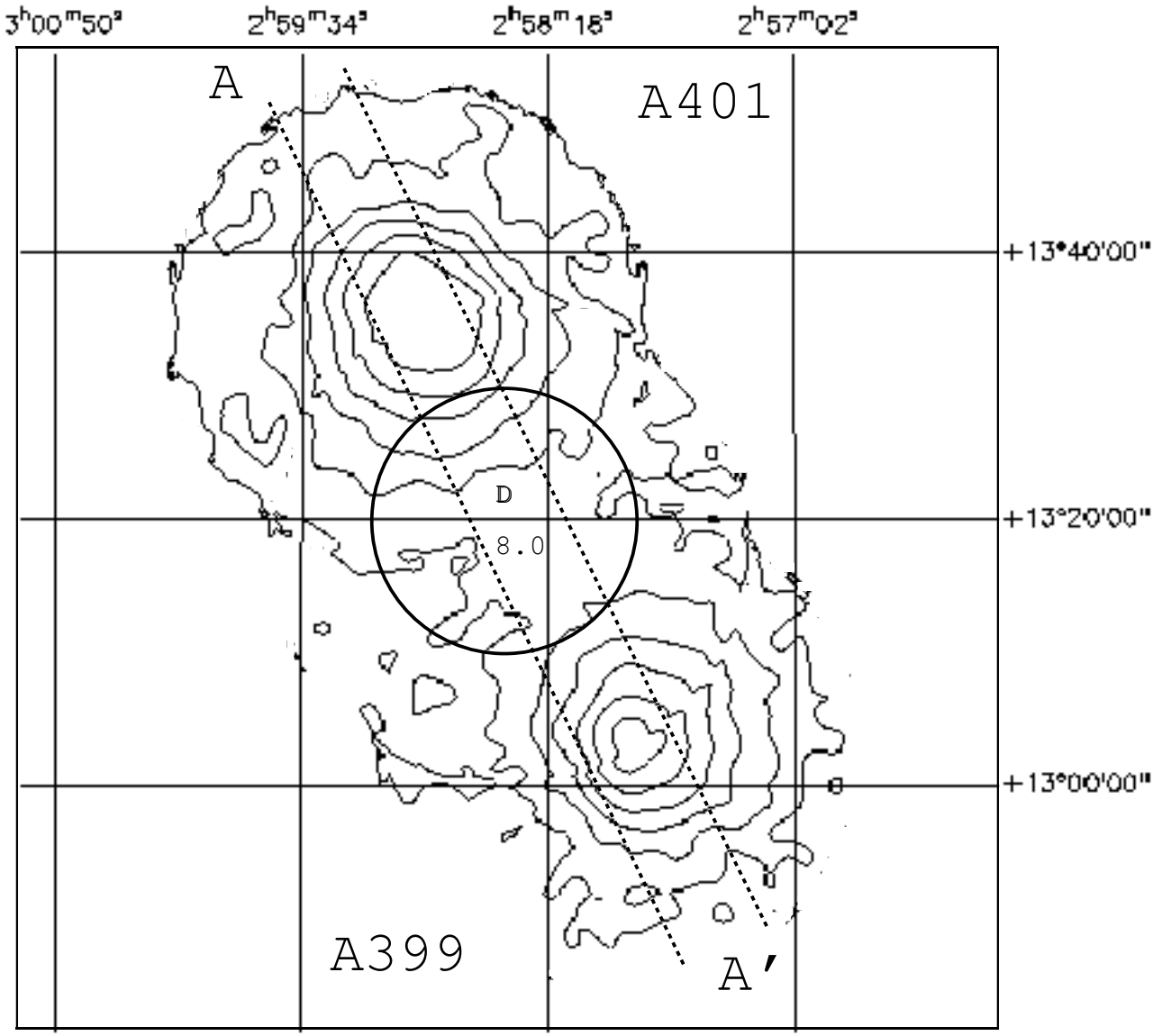
3h00m50s
2h59m34s
2h58m18s
2h57m02s
A
A401
+13°40'00"
+13°20'00"
+13°00'00"
D
8.0
A399
A'

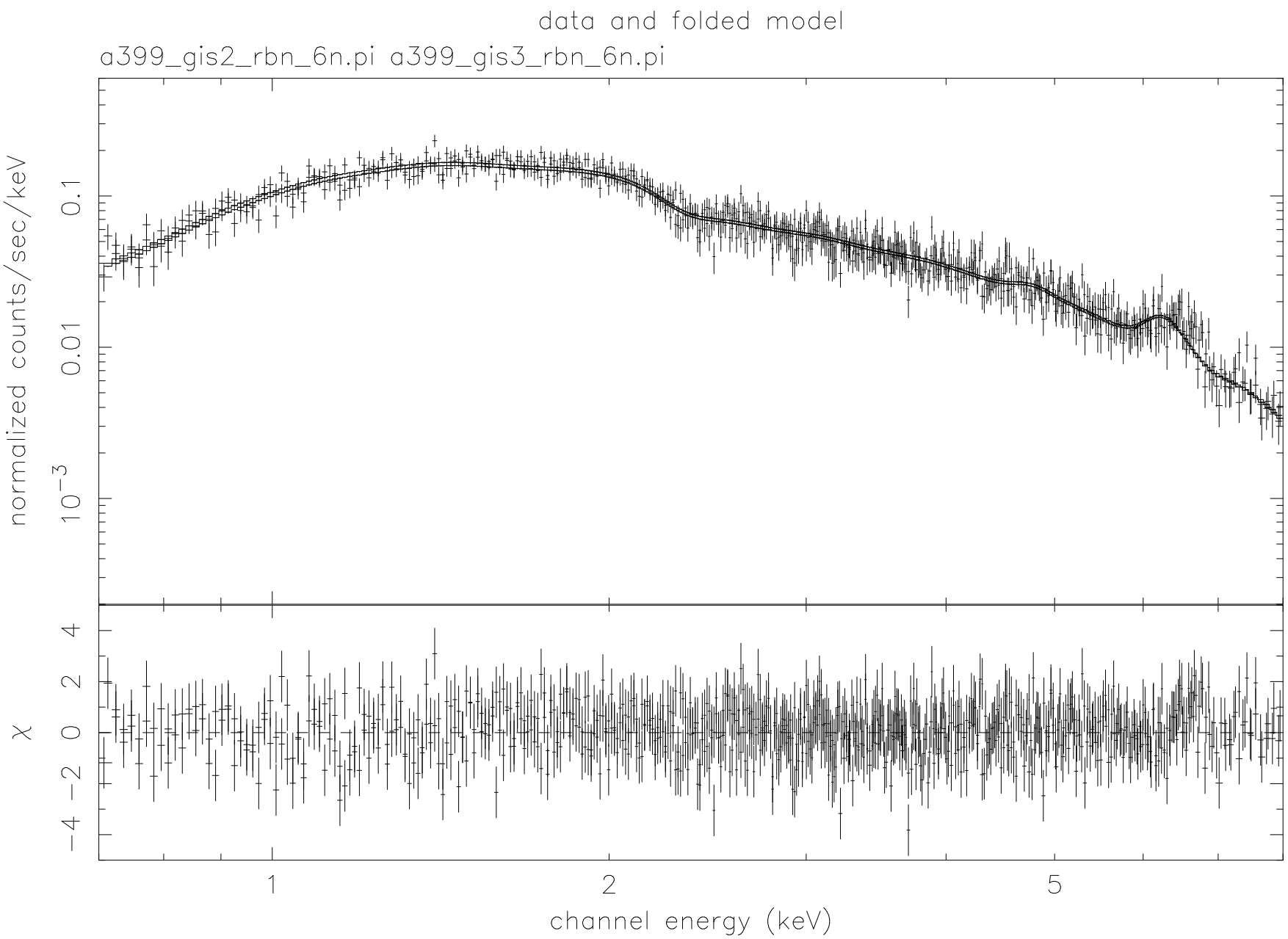
data and folded model
a399_gis2_rbn_6n.pi a399_gis3_rbn_6n.pi
normalized counts/sec/keV
10^{-3}
0.01
0.1
χ
−4 −2 0 2 4
1
2
5
channel energy (keV)

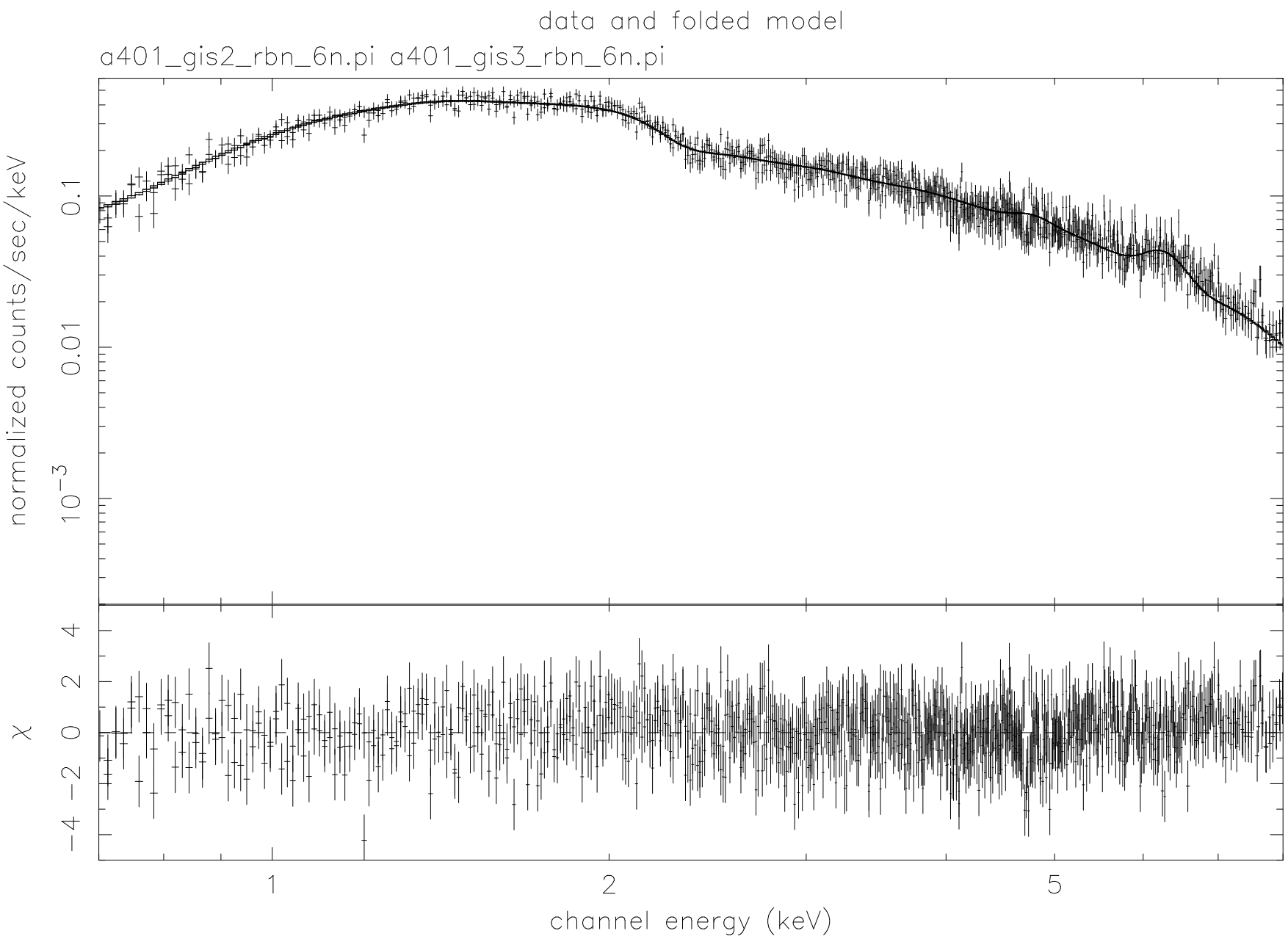
data and folded model
a401_gis2_rbn_6n.pi a401_gis3_rbn_6n.pi
normalized counts/sec/keV
0.1
0.01
10^{-3}
χ
4
2
0
−2
−4
1
2
5
channel energy (keV)

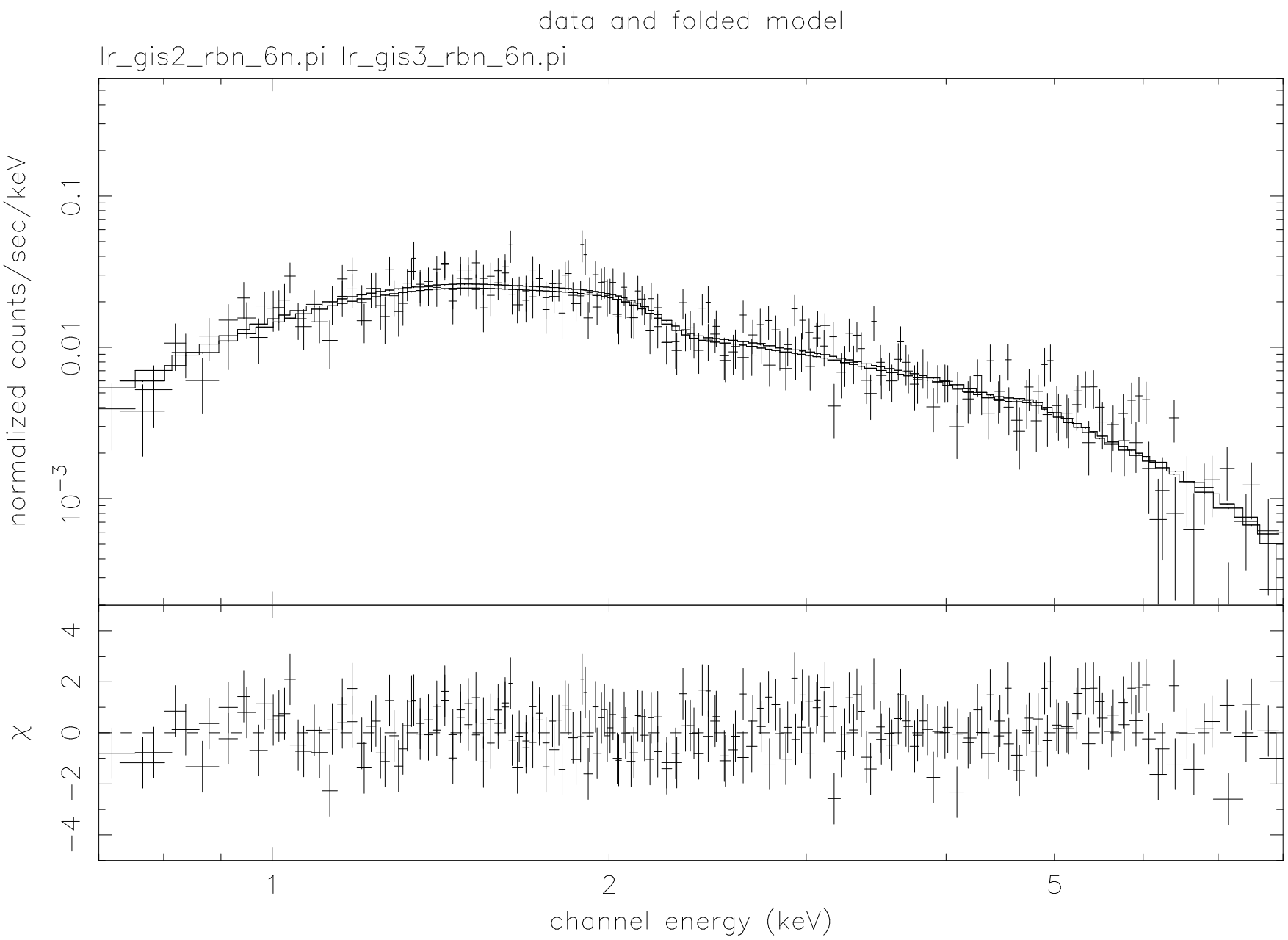
data and folded model
lr_gis2_rbn_6n.pi lr_gis3_rbn_6n.pi
normalized counts/sec/keV
10^{-3}
0.01
0.1
χ
−4 −2 0 2 4
1
2
5
channel energy (keV)

TABLE 2
THE BEST FIT PARAMETERS

	Radius		$0'-1'$	$1'-2'$	$2'-3'$	$3'-4'$	$4'-5'$	$5'-6'$
A399	Temperature	(GIS)	$6.5^{8.4}_{5.1}$	$6.8^{8.3}_{5.8}$	$7.2^{8.7}_{6.1}$	$6.5^{7.6}_{5.6}$	$6.7^{8.2}_{5.6}$	$6.8^{8.4}_{5.6}$
	(keV)	(SIS)	$6.4^{7.5}_{5.5}$	$7.8^{9.0}_{6.8}$	$8.1^{9.3}_{7.0}$	$7.8^{9.0}_{6.8}$	$7.1^{8.0}_{6.3}$	$6.7^{7.7}_{5.8}$
	Abundance	(GIS)	$0.45^{0.69}_{0.22}$	$0.22^{0.35}_{0.09}$	$0.36^{0.50}_{0.22}$	$0.25^{0.39}_{0.12}$	$0.16^{0.30}_{0.02}$	$0.34^{0.53}_{0.16}$
	(solar)	(SIS)	$0.47^{0.71}_{0.25}$	$0.0^{0.10}_{0.0}$	$0.15^{0.25}_{0.04}$	$0.29^{0.42}_{0.18}$	$0.18^{0.29}_{0.08}$	$0.29^{0.42}_{0.16}$
	Absorption	(GIS)	$0.18^{0.27}_{0.09}$	$0.20^{0.27}_{0.14}$	$0.14^{0.20}_{0.08}$	$0.08^{0.14}_{0.02}$	$0.10^{0.16}_{0.03}$	$0.06^{0.13}_{0.0}$
	(10^{22} cm^{-2})	(SIS)	$0.27^{0.31}_{0.23}$	$0.23^{0.26}_{0.21}$	$0.21^{0.24}_{0.18}$	$0.23^{0.26}_{0.20}$	$0.24^{0.26}_{0.21}$	$0.25^{0.28}_{0.22}$
	χ^2/dof	(GIS)	83.62/100	180.6/192	241.5/221	215.3/215	194.5/189	157.9/171
		(SIS)	127.5/123	247.4/200	296.6/229	329.2/227	285.3/215	236.8/198
A401	Temperature	(GIS)	$8.7^{10.5}_{7.3}$	$8.3^{9.4}_{7.3}$	$8.6^{9.8}_{7.6}$	$7.4^{8.6}_{6.6}$	$6.7^{8.2}_{5.6}$	$7.6^{9.0}_{6.5}$
	(keV)	(SIS)	$8.1^{9.7}_{6.8}$	$8.6^{9.5}_{7.7}$	$8.5^{9.4}_{7.6}$	$8.2^{9.1}_{7.3}$	$7.8^{8.8}_{6.9}$	$7.4^{8.5}_{6.7}$
	Abundance	(GIS)	$0.24^{0.38}_{0.11}$	$0.29^{0.40}_{0.20}$	$0.20^{0.29}_{0.11}$	$0.23^{0.32}_{0.14}$	$0.17^{0.26}_{0.07}$	$0.15^{0.24}_{0.04}$
	(solar)	(SIS)	$0.18^{0.34}_{0.02}$	$0.29^{0.38}_{0.20}$	$0.18^{0.27}_{0.09}$	$0.18^{0.26}_{0.09}$	$0.10^{0.18}_{0.01}$	$0.21^{0.32}_{0.11}$
	Absorption	(GIS)	$0.11^{0.16}_{0.06}$	$0.11^{0.15}_{0.07}$	$0.13^{0.17}_{0.09}$	$0.13^{0.17}_{0.08}$	$0.20^{0.25}_{0.16}$	$0.12^{0.18}_{0.07}$
	(10^{22} cm^{-2})	(SIS)	$0.25^{0.28}_{0.22}$	$0.24^{0.26}_{0.22}$	$0.26^{0.28}_{0.24}$	$0.25^{0.27}_{0.23}$	$0.25^{0.27}_{0.23}$	$0.24^{0.27}_{0.22}$
	χ^2/dof	(GIS)	227.1/241	323.0/405	241.5/221	450.7/443	353.8/374	315.9/295
		(SIS)	164.7/165	347.3/256	425.6/283	440.8/278	308.4/259	294.3/235

Note; The numbers next to the best-fit values are the 90% confidence range of the fit.

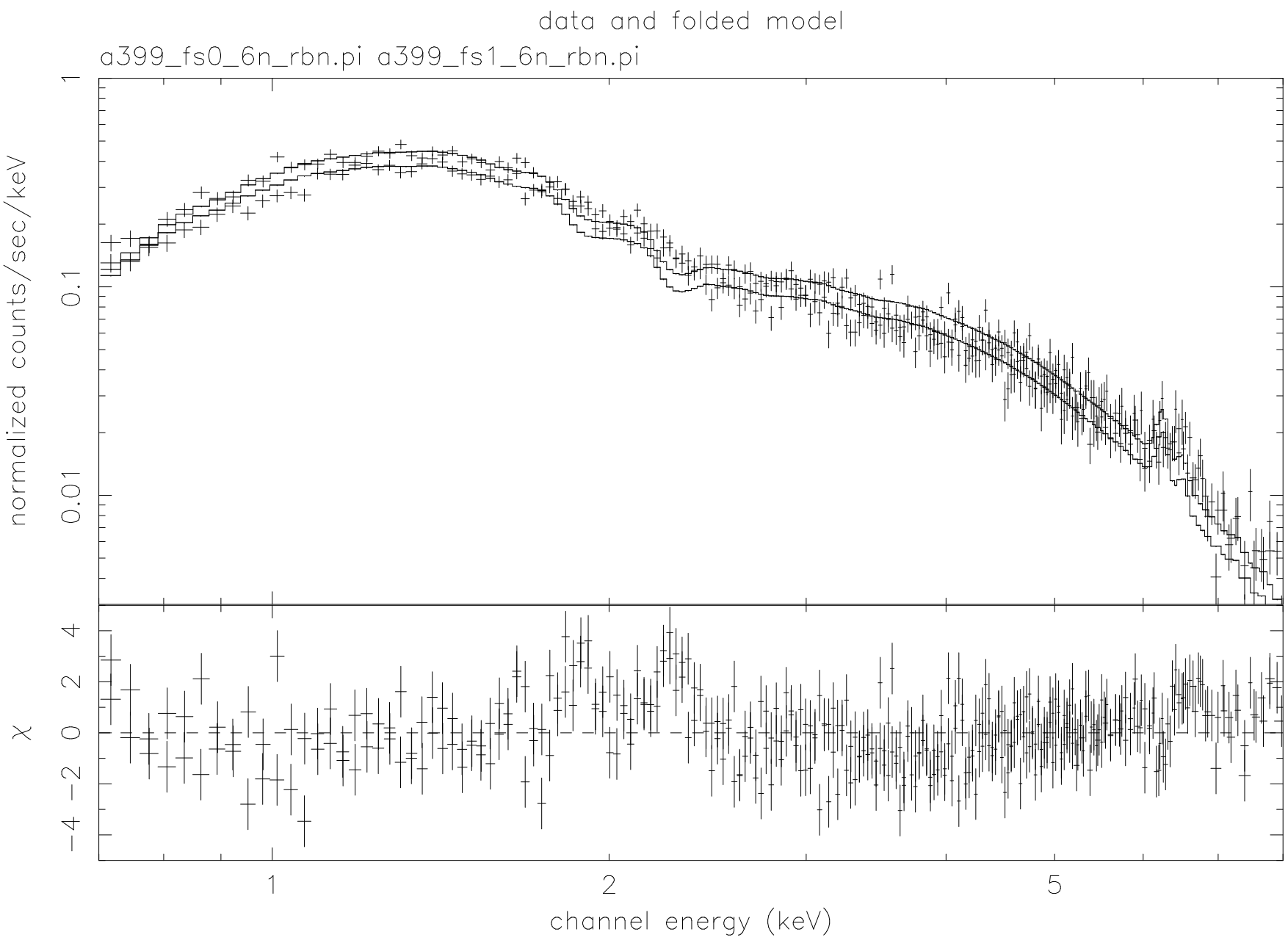
data and folded model
a399_fs0_6n_rbn.pi a399_fs1_6n_rbn.pi
normalized counts/sec/keV
1
0.1
0.01
χ
4
2
0
−2
−4
1
2
5
channel energy (keV)

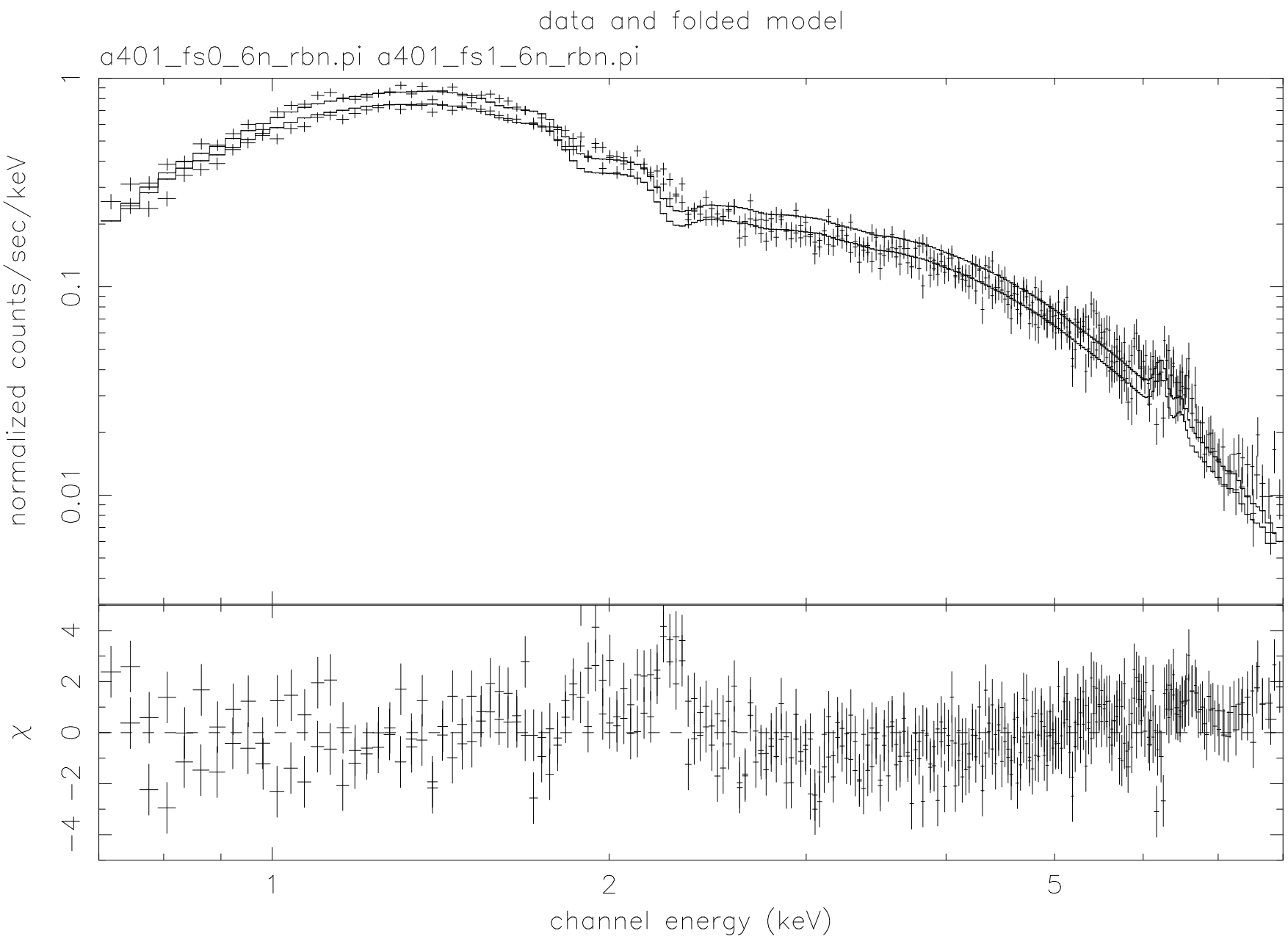
data and folded model
a401_fs0_6n_rbn.pi a401_fs1_6n_rbn.pi
normalized counts/sec/keV
1
0.1
0.01
χ
4
2
0
−2
−4
1
2
5
channel energy (keV)

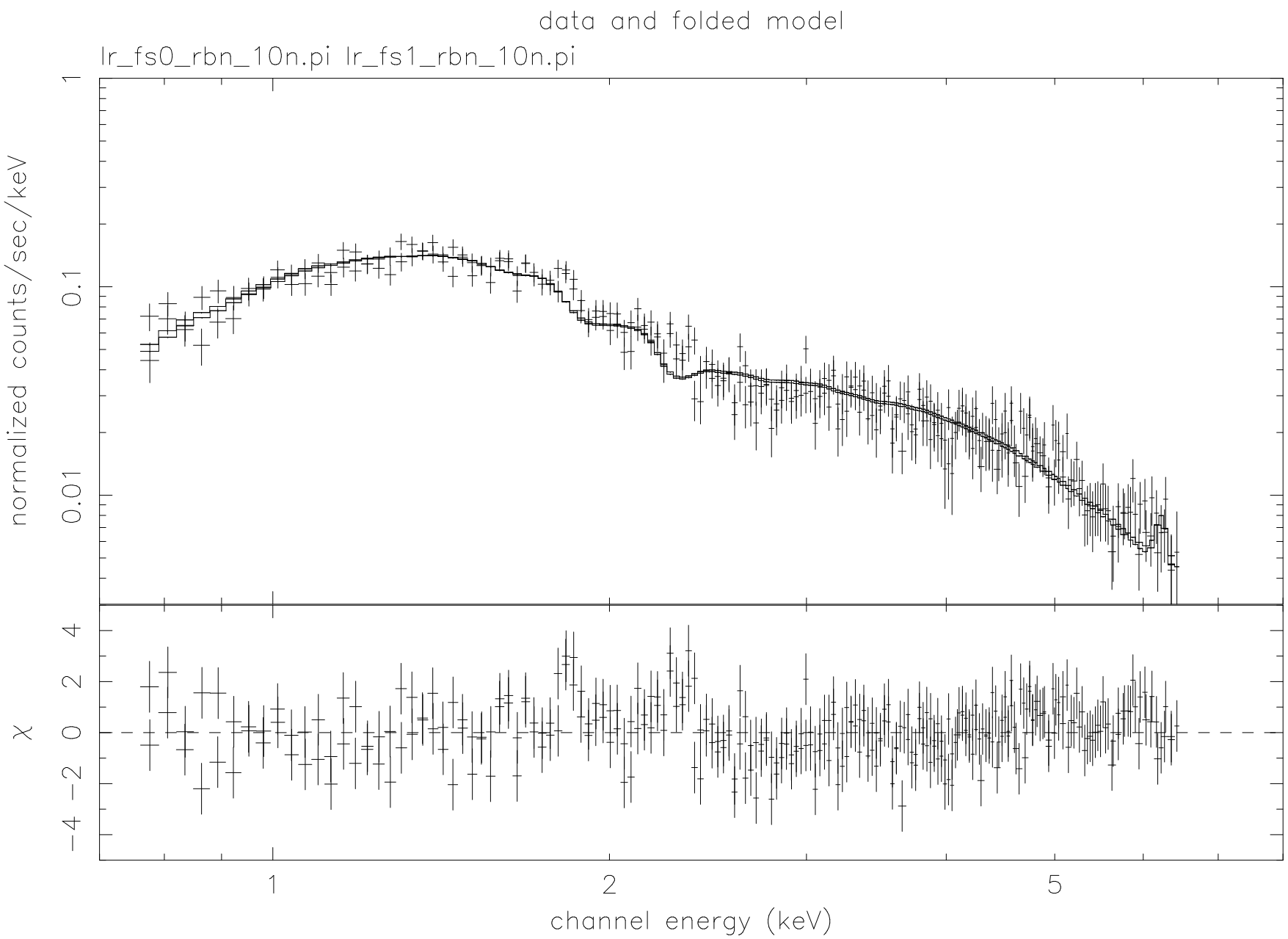
data and folded model
lr_fs0_rbn_10n.pi lr_fs1_rbn_10n.pi
normalized counts/sec/keV
1
0.1
0.01
χ
4
2
0
−2
−4
1
2
5
channel energy (keV)

TABLE 3
THE BEST FIT PARAMETERS

		A0	A1	A2	A3	A4
Temperature	(GIS)	$6.9^{7.3}_{6.5}$	$5.8^{7.3}_{4.7}$	$8.8^{11.6}_{7.0}$	$7.8^{9.7}_{6.3}$	$10.7^{18.2}_{7.1}$
(keV)	(SIS)	$7.8^{8.3}_{7.3}$	...	...	...	...
Abundance	(GIS)	$0.25^{0.30}_{0.20}$	$0.04^{0.22}_{0.0}$	$0.28^{0.50}_{0.07}$	$0.28^{0.44}_{0.12}$	$0.0^{0.28}_{0.0}$
(solar)	(SIS)	$0.19^{0.23}_{0.13}$	...	...	...	...
Absorption	(GIS)	$0.08^{0.11}_{0.06}$	$0.21^{0.12}_{0.31}$	$0.08^{0.16}_{0.02}$	$0.10^{0.17}_{0.03}$	$0.27^{0.42}_{0.14}$
(10^{22} cm^{-2})	(SIS)	$0.22^{0.23}_{0.21}$	...	...	...	...
2-10 keV flux	(GIS)	17.0	2.8	4.2	4.3	1.8
(10^{-12}erg cm^{-2}s^{-1})	(SIS)	19.7	...	...	...	...
χ^2/dof	(GIS)	814.7/821	244.7/214	255.3/253	249.2/279	178.9/175
	(SIS)	683.9/396	...	...	...	...
		B0	B1	B2	B3	B4
Temperature	(GIS)	$8.0^{8.4}_{7.5}$	$11.2^{15.2}_{8.9}$	$8.9^{11.0}_{7.3}$	$8.4^{9.9}_{7.1}$	$9.6^{12.3}_{7.8}$
(keV)	(SIS)	$8.3^{8.8}_{7.8}$	...	...	...	...
Abundance	(GIS)	$0.21^{0.25}_{0.17}$	$0.27^{0.48}_{0.06}$	$0.26^{0.41}_{0.10}$	$0.10^{0.21}_{0.0}$	$0.47^{0.69}_{0.28}$
(solar)	(SIS)	$0.13^{0.09}_{0.16}$	...	...	...	...
Absorption	(GIS)	$0.12^{0.14}_{0.11}$	$0.04^{0.10}_{0.0}$	$0.12^{0.18}_{0.06}$	$0.09^{0.14}_{0.04}$	$0.13^{0.19}_{0.06}$
(10^{22} cm^{-2})	(SIS)	$0.26^{0.27}_{0.25}$	...	...	...	...
2-10 keV flux	(GIS)	38.0	3.5	5.2	6.7	3.7
(10^{-12}erg cm^{-2}s^{-1})	(SIS)	42.6	...	...	...	...
χ^2/dof	(GIS)	1061/1011	272.3/300	334.3/332	400.3/416	321.4/308
	(SIS)	760.6/426	...	...	...	...
		C1	C0	C2	D	
Temperature	(GIS)	$6.4^{7.3}_{5.6}$	$7.9^{10.0}_{6.4}$	$7.4^{8.1}_{6.9}$	...	
(keV)	(SIS)	...	...	...	$8.0^{9.1}_{7.0}$	
Abundance	(GIS)	$0.09^{0.19}_{0.0}$	$0.0^{0.10}_{0.0}$	$0.28^{0.35}_{0.22}$	...	
(solar)	(SIS)	...	...	...	$0.17^{0.08}_{0.27}$	
Absorption	(GIS)	$0.09^{0.14}_{0.05}$	$0.14^{0.21}_{0.07}$	$0.13^{0.15}_{0.10}$	...	
(10^{22} cm^{-2})	(SIS)	...	...	...	$0.27^{0.29}_{0.23}$	
2-10 keV flux	(GIS)	10.0	0.7	39.5	...	
(10^{-12}erg cm^{-2}s^{-1})	(SIS)	...	...	...	11.6	
χ^2/dof	(GIS)	399.0/447	231.5/230	660.8/707	...	
	(SIS)	...	...	...	376.4/324	

Note; The numbers next to the best-fit values are the 90% confidence range of the fit.

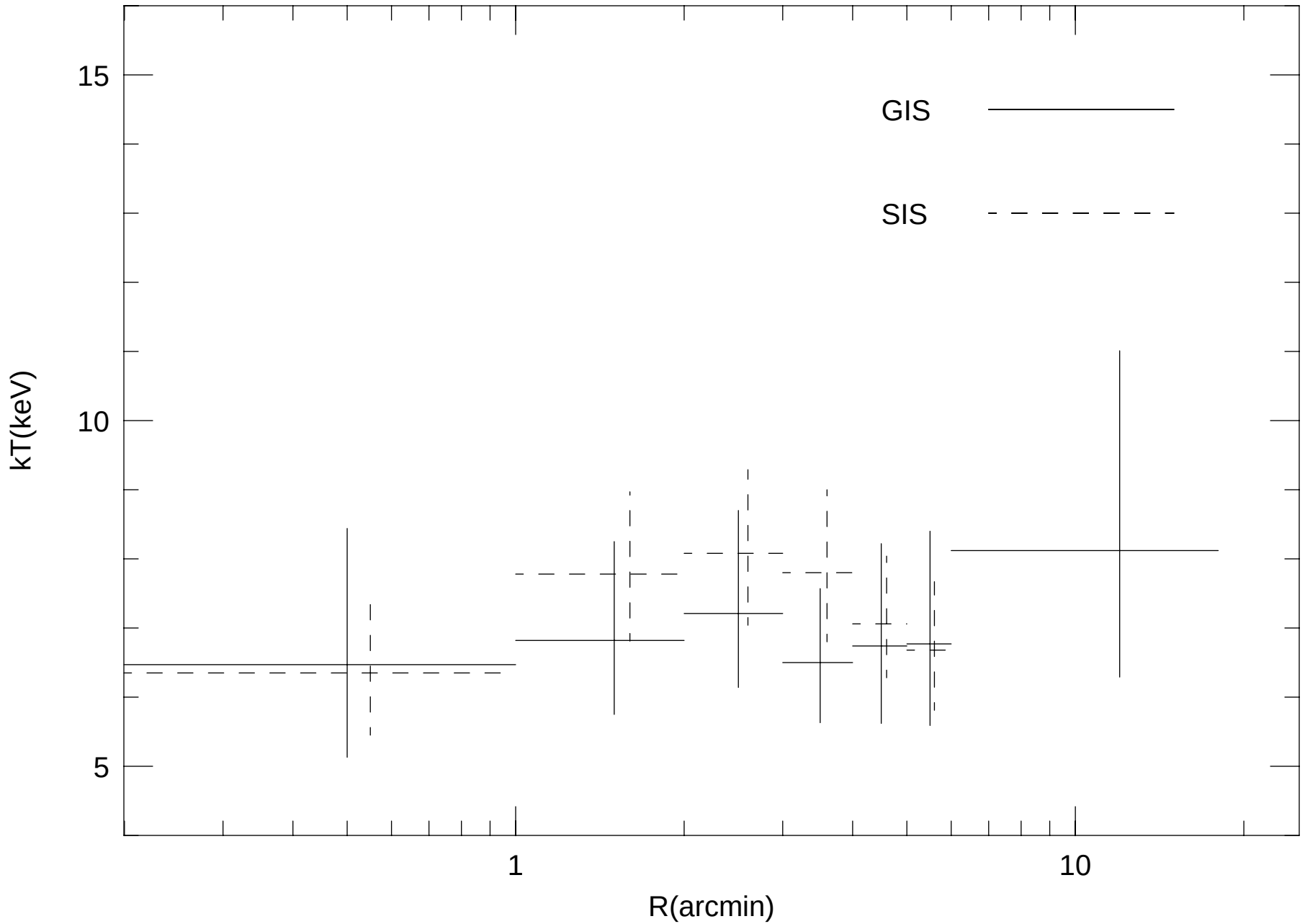
15
10
5
kT(keV)
GIS
SIS
1
10
R(arcmin)

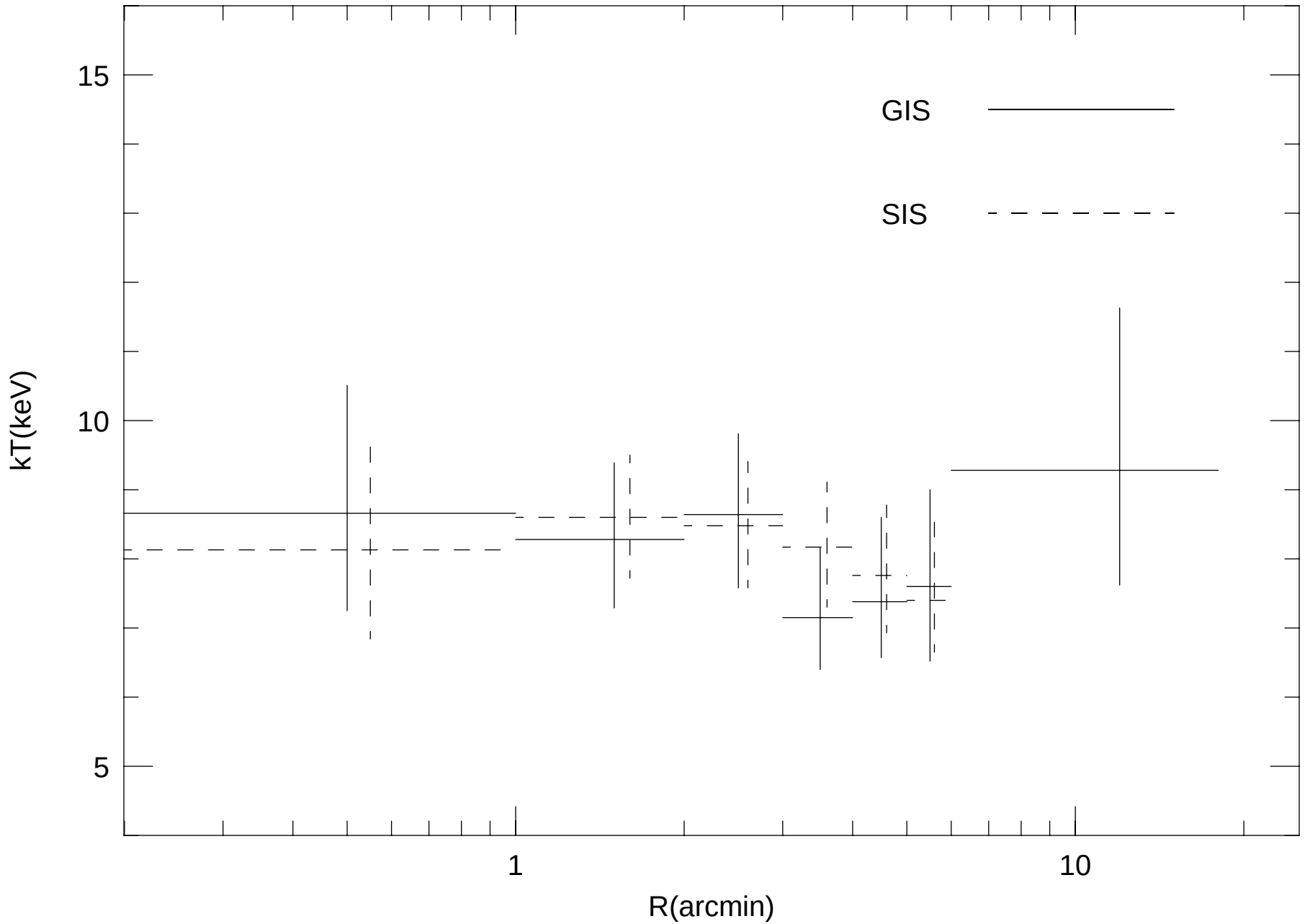
15
10
5
kT(keV)
GIS
SIS
1
10
R(arcmin)

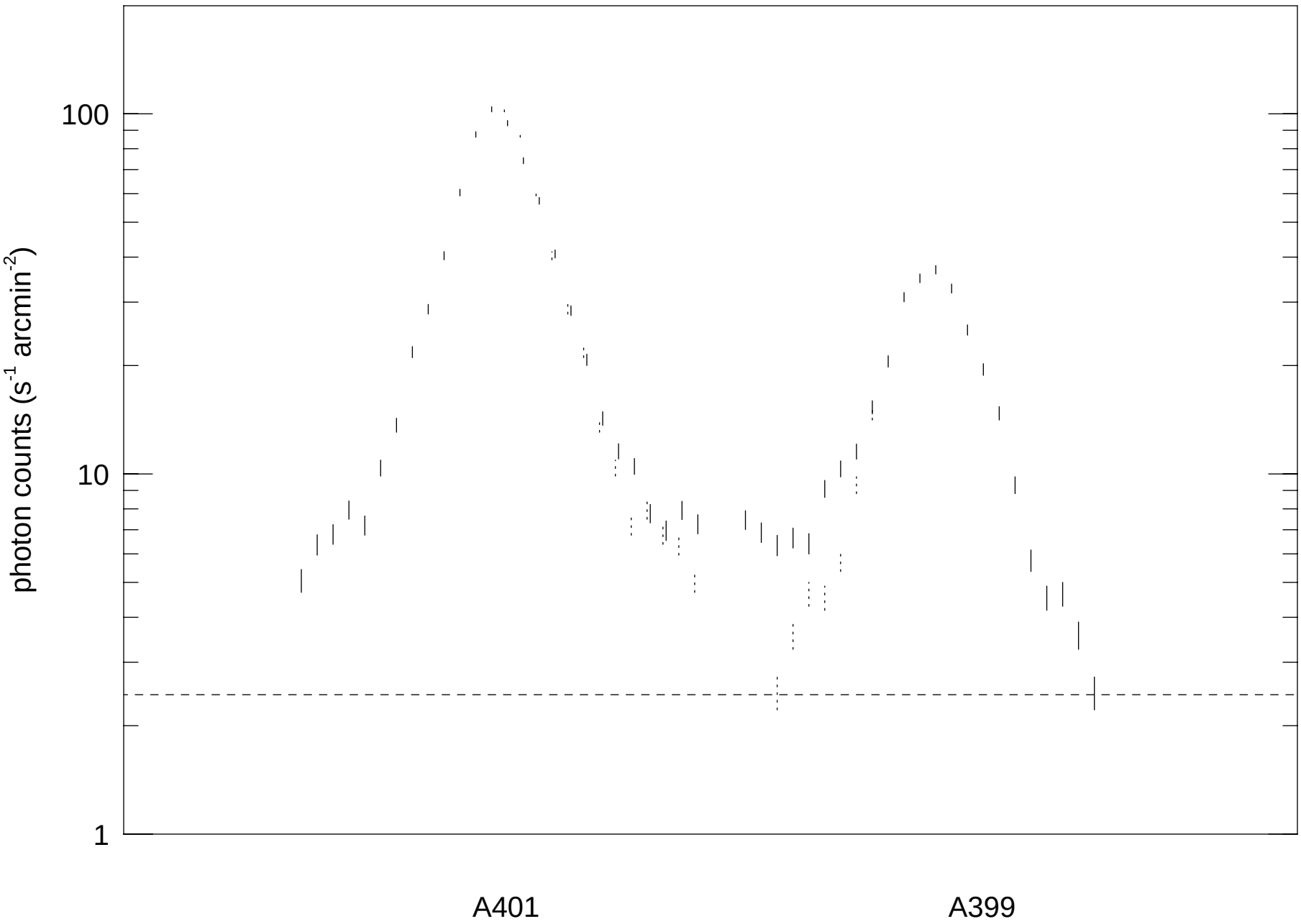
100
10
1
photon counts (s-1 arcmin-2)
A401
A399

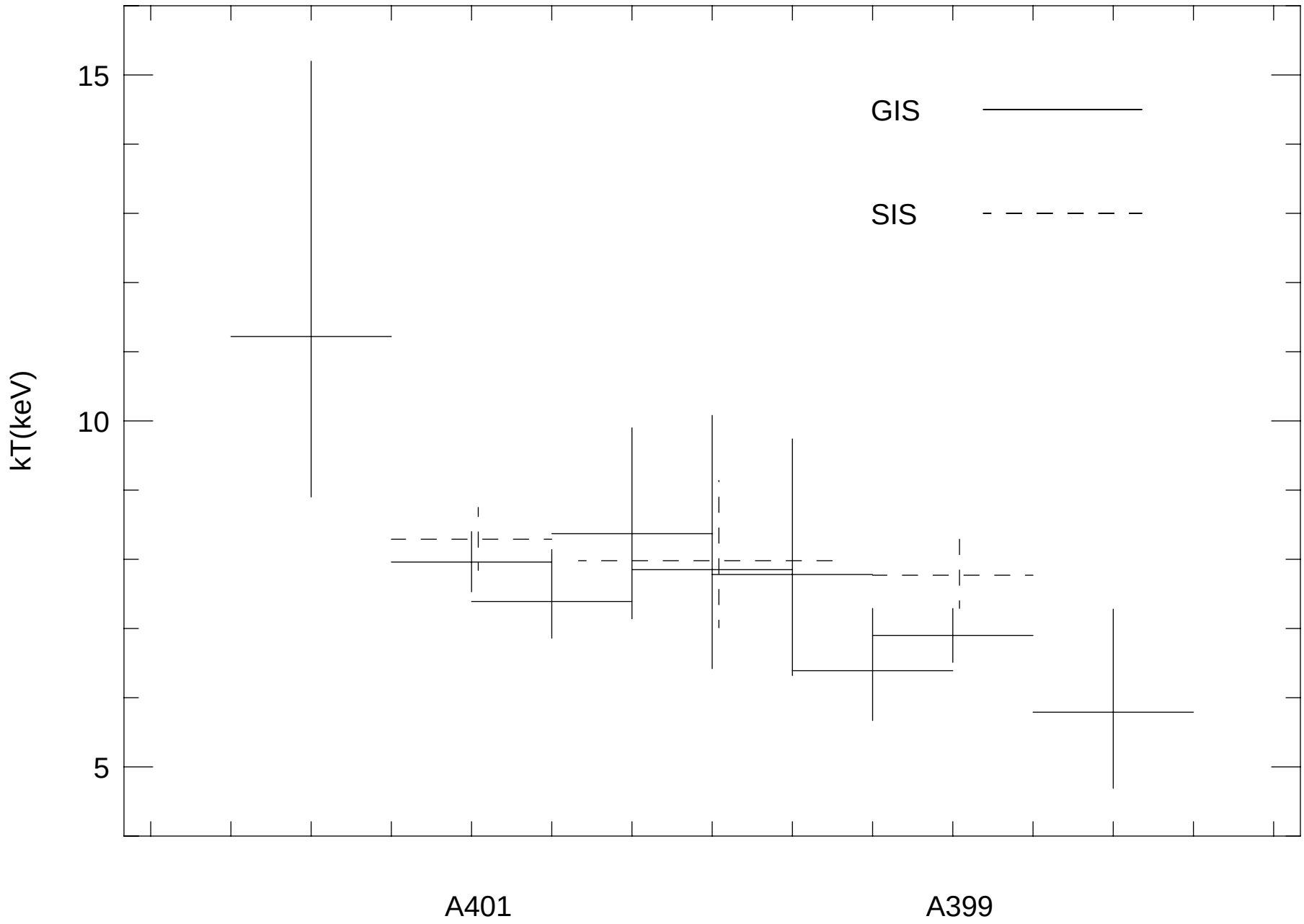
15
10
5
kT(keV)
GIS
SIS
A401
A399